Framework for simulating stationary spherical flames

Fernando Ruiz^{a,*}, Guillaume Beardsell^a, Guillaume Blanquart^a

^aDepartment of Mechanical Engineering, California Institute of Technology, Pasadena, USA

Abstract

Understanding and quantifying the effects of flame stretch rate on the laminar flame speed and flame structure plays an important role from interpreting experimentally-measured laminar burning velocities to characterizing the impact of turbulence on premixed flames. Unfortunately, accounting for these effects often requires an unsteady reacting flow solver and may be computationally expensive. In this work, we propose a mathematical framework to perform simulations of stationary spherical flames. The objective is to maintain the flame at a constant radius (and hence a constant stretch rate) by performing a coordinate change. The governing equations in the new flame-attached frame of reference resemble the original equations for freely-propagating spherical flames. The only difference is the presence of additional source terms whose purpose is to drive the numerical solution to a steady state. These source terms involve one free parameter: the flame stretch rate, which may either be computed in real time or imposed by the user. This parameter controls ultimately the steady state flame radius and the steady state flame speed. That is why, at a given stretch rate, the results of the stationary spherical flame simulations match those of a freely-expanding spherical flame. As an illustration, the dependence of the laminar flame speed on the stretch rate is leveraged to extract Markstein lengths for hydrogen/air mixtures at different equivalence ratios, as well as for hydrocarbon/air mixtures (CH₄ and C₇H₁₆). Numerical predictions are in good agreement with experimental measurements (within experimental uncertainties).

Finally, the proposed methodology is implemented in the chemical kinetic software FlameMaster. The use of a dedicated steady-state solver with a non-uniform optimized mesh leads to significant reductions in the computational cost, highlighting that the proposed methodology is ideally suited for other chemical kinetic software such as Chemkin/Premix and Cantera.

Keywords:

Laminar flame speed, Markstein length, Stretched flames, Steady-state solver

^{*}Corresponding author:

1. Introduction

The development of detailed chemical kinetic models relies on extensive validation of the model's performance against experimental measurements (e.g. [1, 2]). The most commonly-used configurations for this validation include shock tubes, plug flow reactors, jet-stirred reactors, premixed flames, and counterflow diffusion flames. One-dimensional premixed flames are the simplest and most canonical configuration that includes a balance between chemical reaction and species diffusion. The quantity of interest, the unstretched laminar flame speed (or burning velocity), S_L^0 , has been measured for a variety of fuels, equivalence ratios, unburnt temperatures, and background pressures.

Various experimental setups have been proposed for measuring the laminar flame speed including Bunsen flames [3], twin counterflow flames [4], heat flux methods [5], and freely-expanding spherical flames [6]. Each of these methods has their own advantages and challenges. The present work focuses on the spherically-expanding flame configuration as it has been used successfully for atmospheric as well as high pressure measurements.

The combination of flame curvature and strain rate of the unburnt velocity field causes the structure and behavior of spherical flames to deviate from their flat flame counterparts. These stretch effects are often quantified through the flame stretch rate [7]

$$\kappa = \frac{1}{A} \frac{dA}{dt} = \frac{2}{r_F} \frac{dr_F}{dt} \,. \tag{1}$$

where A is the flame surface area, and r_F is the flame radius.

First discussed by Markstein [8], the dependence of the laminar flame speed on the stretch rate has been the subject of a considerable body of work using asymptotic analysis yielding both linear and non-linear expressions [9–13]. These expressions have been tested in numerical simulations [14, 15] and experimental measurements [4, 16, 17]. The analysis has also been extended to turbulent premixed flames [18, 19]. It is commonly accepted that in the limit of small stretch rates κ , the flame speed, S_L , is well approximated by

$$\frac{S_L}{S_L^0} = 1 - \frac{\mathcal{L}_M}{S_L^0} \kappa,\tag{2}$$

where \mathcal{L}_M is the Markstein length. Unfortunately, experimental measurements are often made at finite stretch rates, and the above expression may not be valid to extrapolate to zero stretch rate. Many studies have

been dedicated to the uncertainty of such extrapolations (e.g. [15, 20]).

These studies point out to the need to perform unsteady numerical simulations of spherically expanding flames with detailed chemistry to evaluate explicitly the dependence of the laminar flame speed on the stretch rate. This serves the dual purpose of providing a more accurate extrapolation to zero stretch rate as well as evaluating the Markstein length scale. However, these simulations present their own challenges. First, most (if not all of the) numerical software used to develop and validate detailed kinetic models only include a steady-state solver for unstretched premixed flames Chemkin [21], Cantera [22], and FlameMaster [23]). Second, the existing unsteady solvers with detailed chemistry are often used to simulate only a small range of stretch rates, as zero stretch rate is mathematically unreachable (it corresponds to an infinite radius).

The intent of the present work is not to propose yet another extrapolation method for the laminar flame speed to zero stretch rate, or to provide specific insight into the physics of spherical premixed combustion. The objective is to propose a numerical framework to simulate one-dimensional *stretched* laminar flames using a *steady-state* solver. The proposed simulation framework could then be used to accelerate the processing of experimental data, to evaluate Markstein lengths from detailed kinetic models, and to provide insight into the effects of strain rate and curvature on turbulent premixed flames. This work differs from other studies [24] in which *stationary* spherical flames were simulated, i.e., for which κ was set to zero (dA/dt = 0).

The paper is organized as follows. In Section 2, we present the governing equations for freely expanding spherical flames and derive the new governing equations for stationary spherical flames following a coordinate change. We also provide an analytical closure for the flame stretch rate, κ . Then, the numerical setup is reviewed in Section 3, and a series of validation tests is presented in Section 4 for a hydrogen/air mixture at an equivalence ratio $\phi = 0.4$. Section 5 covers a detailed explanation of stretch effects, including the extraction of the Markstein length for a variety of equivalence ratios and fuels (hydrogen, methane and n-heptane) at standard conditions. Finally, the proposed framework is implemented in the steady-state solver FlameMaster, and a computational cost analysis is presented.

2. Methodology

Two sets of simulations will be performed, namely freely-expanding spherical flames and stationary spher-

ical flames. The equations for each case are described first, followed by a discussion of the closure problem.

2.1. Freely-expanding spherical flame equations

The set of equations for a one-dimensional, freely-propagating, spherical flame under the low Mach number approximation consists of conservation of mass, transport equations for each of the species mass fractions, and the temperature equation

$$\frac{\partial \rho}{\partial t} + \frac{1}{r^2} \frac{\partial r^2 \rho u_r}{\partial r} = 0, \qquad (3)$$

$$\frac{\partial \rho Y_k}{\partial t} + \frac{1}{r^2} \frac{\partial r^2 \rho Y_k u_r}{\partial r} = -\frac{1}{r^2} \frac{\partial}{\partial r} \left(r^2 j_k \right) + \dot{\omega}_k , \quad (4)$$

$$\rho c_p \left[\frac{\partial T}{\partial t} + u_r \frac{\partial T}{\partial r} \right] = \frac{1}{r^2} \frac{\partial}{\partial r} \left(r^2 \lambda \frac{\partial T}{\partial r} \right) - \sum_{k=1}^{n_s} c_{p,k} j_k \frac{\partial T}{\partial r} + \dot{\omega}_T .$$
(5)

The governing equations in the spatial radial coordinate r, are solved to extract the radial velocity, u_r , pressure, p, density, ρ , temperature, T, and the n_s species mass fractions, Y_k . j_k is the diffusion flux of species k, $\dot{\omega}_k$ is its chemical production term, and $\dot{\omega}_T$ is the heat release rate. c_p is the mixture heat capacity at constant pressure, and λ is the thermal conductivity. Finally, the ideal gas law is used to close the system

$$\rho = \frac{p_0 W}{RT} \,. \tag{6}$$

where R is the universal gas constant, W is the molar mass of the mixture, and p_0 is the background pressure.

2.2. Stationary spherical flames

We perform a coordinate change to seek a stationary solution in a flame-attached frame of reference.

2.2.1. Coordinate change

We introduce a flame-attached frame of reference defined by $r' = r \cdot \frac{r_0}{r_F(t)}$ and t' = t, where $r_0 = r_F(t_0)$ is the initial flame radius. This leads to the following set of equations.

$$\frac{\partial \rho}{\partial t'} + \frac{r_0}{r_F} \frac{1}{r'^2} \frac{\partial r'^2 \rho u_r}{\partial r'} = \frac{\dot{r}_F}{r_F} r' \frac{\partial \rho}{\partial r'}, \qquad (7)$$

$$\frac{\partial \rho Y_k}{\partial t'} + \frac{r_0}{r_F} \frac{1}{r'^2} \frac{\partial r'^2 \rho Y_k u_r}{\partial r'} = -\frac{r_0^2}{r_F^2} \frac{1}{r'^2} \frac{\partial r'^2 j'_k}{\partial r'} + \frac{\dot{r}_F}{r_F} r' \frac{\partial \rho Y_k}{\partial r'} + \dot{\omega}_k ,$$
(8)

$$\rho c_{p} \left[\frac{\partial T}{\partial t'} + \frac{r_{0}}{r_{F}} u_{r} \frac{\partial T}{\partial r'} \right] = \frac{r_{0}^{2}}{r_{F}^{2}} \frac{1}{r'^{2}} \frac{\partial}{\partial r'} \left(r'^{2} \lambda \frac{\partial T}{\partial r'} \right) + \rho c_{p} \frac{\dot{r}_{F}}{r_{F}} r' \frac{\partial T}{\partial r'} - \frac{r_{0}^{2}}{r_{F}^{2}} \sum_{k=1}^{n_{s}} c_{p,k} j'_{k} \frac{\partial T}{\partial r'} + \dot{\omega}_{T}, \quad (9)$$

We note that the ratio \dot{r}_F/r_F is nothing more than half the flame stretch rate, κ , of a freely-propagating flame (see Eq. 1). An analytical closure for this flame stretch rate will be presented in section 2.2.2.

Assuming the coordinate transformation is successful, the flame in the new coordinate system is stationary. In other words, the flame radius remains at its initial value, $r_F = r_0$, and Eq 7-9 become

$$\frac{\partial \rho}{\partial t'} + \frac{1}{r'^2} \frac{\partial r'^2 \rho u_r}{\partial r'} = \frac{\kappa}{2} r' \frac{\partial \rho}{\partial r'}, \qquad (10)$$

$$\frac{\partial \rho Y_k}{\partial t'} + \frac{1}{r'^2} \frac{\partial r'^2 \rho Y_k u_r}{\partial r'} = -\frac{1}{r'^2} \frac{\partial r'^2 j'_k}{\partial r'} + \frac{\kappa}{2} r' \frac{\partial \rho Y_k}{\partial r'} + \dot{\omega}_k,$$
(11)

$$\rho c_{p} \left[\frac{\partial T}{\partial t'} + u_{r} \frac{\partial T}{\partial r'} \right] = \frac{1}{r'^{2}} \frac{\partial}{\partial r'} \left(r'^{2} \lambda \frac{\partial T}{\partial r'} \right) + \rho c_{p} \frac{\kappa}{2} r' \frac{\partial T}{\partial r'} - \sum_{k=1}^{n_{s}} c_{p,k} j'_{k} \frac{\partial T}{\partial r'} + \dot{\omega}_{T}. \quad (12)$$

These unsteady equations resemble the initial set of equations for freely expanding flames (Eq. 3-5). The only difference is the presence of additional source terms on the right hand side. These additional metric source terms allow our governing equations (Eq. 10 - 12) for a stationary flame to directly correspond with the freely expanding flame.

2.2.2. Calculation of κ

The objective is to calculate in real time the flame stretch rate, κ , necessary to force a steady state at the initial flame radius. Such value is the eigenvalue for the steady-state solution of Eq. 10-12.

We start by integrating the global mass conservation equation (Eq. 10) over the whole domain (from r' = 0 to r' = R) assuming a steady state. This leads to the evaluation of the outlet radial velocity

$$u_{r,\infty} = \frac{\kappa}{2} \left[R - 3 \int \frac{\rho}{\rho_u} \left(\frac{r'}{R} \right)^2 dr' \right]. \tag{13}$$

Then, we integrate any of the species transport equations (Eq. 11) over the whole domain. Leveraging the fact the diffusion fluxes are zero at r' = 0 (because of

symmetry) and at r' = R (far away in the unburnt side), we obtain

$$\kappa = \frac{2\int \dot{\omega}_k r'^2 dr'}{\int 3\rho(Y_k - Y_{k,u})r'^2 dr'},$$
 (14)

Theoretically, this expression can be evaluated for any species (reactants, products, or intermediates) at each time step within the simulation to enforce temporal stationarity.

2.2.3. Closure estimates

We now seek a priori estimates for the value of κ . As a first approximation, we consider infinitely thin flames, and use the fuel as the representative species. Under these assumptions, the numerator of Eq. 14 is related to the laminar burning speed (Eq. 19), and the denominator is related to the total mass of burnt gas. We obtain the following algebraic equation

$$\kappa_{est}^{(1)} = 2 \frac{\rho_u}{\rho_b} \frac{S_L}{r_F} \,, \tag{15}$$

with ρ_b and ρ_u the density of the burnt and unburnt gas, respectively. This first estimate provides an upper bound since it underestimates the mass of burnt gases. We can improve it by considering not only the fully burnt gases (between r'=0 and $r'=r_F$) but also the burnt gases within the flame front itself (between $r'=r_F$ and $r'=r_F+l_F$), where l_F is the flame thickness (see Eq. 18). Poinsot and Veynante proposed the following expression [25]

$$\kappa_{est}^{(2)} = 2 \frac{\rho_u}{\rho_b} \frac{S_L}{r_F} \left[1 + \frac{l_F}{2r_F} \left(1 + \frac{\rho_u}{\rho_b} \right) \right]^{-1},$$
(16)

This second estimate was obtained by assuming mean values for all variables within the flame zone, and provides a 'correction term' for the zero flame thickness results. For large spherical flames, $r_F \gg l_F$, the first approximation is recovered. We discuss the precision of these two estimates in Section 4.

3. Numerical Setup

All numerical simulations are performed using the energy conservative, finite-difference, low-Mach number solver NGA [26] which is second-order accurate in time. In space, we use the BQUICK scheme for species advection [27] and second-order centered difference schemes for the other discretization and interpolation operators. We use 1200 uniformly spaced grid points, corresponding to about 20 points per flame

thickness. Finally, we apply shear-free boundary conditions at the outlet (Neumann boundary conditions) and a symmetry condition at the centerline.

We use a mixture-averaged formulation to compute the species diffusion fluxes [28]. The species viscosities, μ_i , are obtained from standard gas kinetic theory [29], and the mixture-averaged viscosity, μ , is calculated using a modified form of Wilke's formula [30]. The species thermal conductivities, λ_i , are evaluated using a modified version of Eucken's formula [31]. The mixture-averaged thermal conductivity, λ , is computed following Mathur et al. [32].

The chemistry model used for hydrogen is the 9 species, 54 reactions mechanism by Hong et al. [33], for which some of the rate constants have recently been updated [34, 35]. The well-established GRI-Mech 3.0 mechanism [1], which includes 52 species and 634 reactions, is used for methane. Finally, for n-heptane, the model used is the reduced mechanism of Bisetti et al. [36], which contains 47 species and 290 reactions. All simulations are performed at standard conditions ($T_u = 298$ K and $p_0 = 1$ atm). Serving as the basis for the validation process, Figure 1 shows a comparison of the predicted unstretched laminar flame speeds with experimental data for hydrogen/air mixtures (results obtained with FlameMaster [23]).

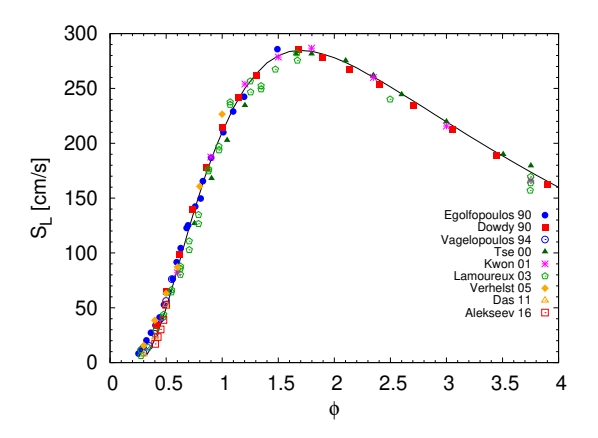
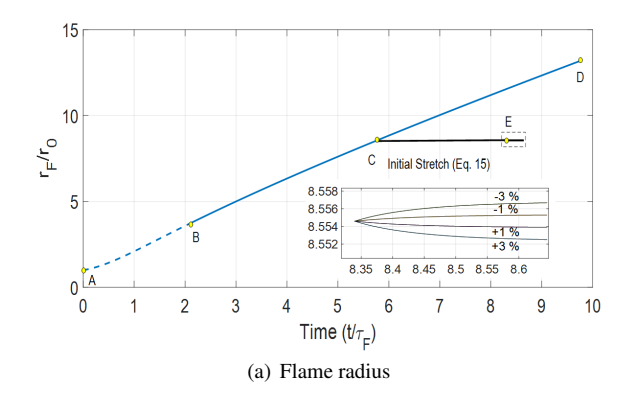


Figure 1: Comparison of one-dimensional unstretched laminar flame speeds with experimental measurements for hydrogen-air mixtures [37–41]

Several global quantities will be evaluated from the unsteady simulations. Multiple definitions of flame radius and flame speed exist [42, 43]. In this work, the flame radius is defined from the volume integral of the fuel density

$$r_F = \sqrt[3]{R^3 - \frac{1}{\frac{4}{3}\pi\rho_u Y_{F,u}} \int_V \rho Y_F dV}.$$
 (17)



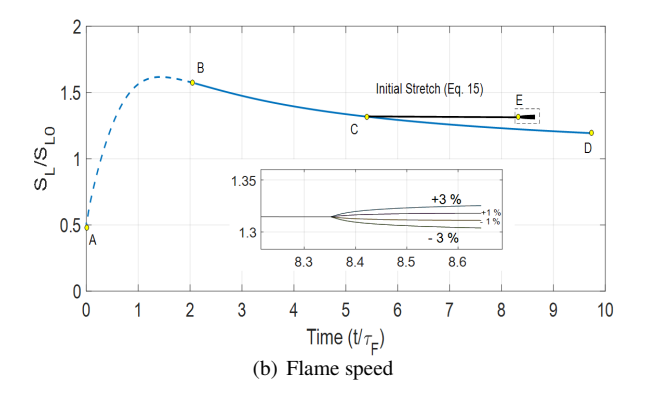


Figure 2: Time evolution of the normalized flame radius (left) and flame speed (right) for the validation case ($\phi = 0.4$). The results for the freely-propagating spherical flame (Eq. 3-5) are shown with blue lines and for the stationary spherical flame (Eq. 10-12) with black lines.

The flame thickness is defined from the maximum gradient of the temperature profile as

$$l_F = \frac{T_b - T_u}{\max\left(\frac{dT}{dr}\right)}. (18)$$

where T_u and T_b are the unburnt and burnt temperatures, respectively. The laminar flame speed S_L is defined from the volumetric integral of the fuel reaction rate per unity of flame front surface area,

$$S_L = \frac{1}{\rho_u Y_{F,u} 4\pi r_F^2} \int_V \rho \dot{\omega}_F dV. \tag{19}$$

where $Y_{F,u}$ is the fuel mass fraction in the unburnt, $\dot{\omega}_F$ is the fuel consumption rate, and r_F is obtained from Eq. (17). Note that the choice of a definition for r_F impacts the definition of the flame speed, and hence its dependence on κ [44].

Finally, we define a characteristic time, $\tau_F = l_F^0/S_L^0$, as the time needed for the flame front to travel a distance corresponding to its flame thickness. The superscript 0 refers to values for the unstretched flat flames.

4. Validation

The validation of the proposed numerical framework follows a multi-step approach and is done for a hydrogen/air mixture at $\phi = 0.4$. Figure 2 shows the temporal evolution of the flame radius and flame speed.

The first step involves running a flat flame (1D unstretched) to obtain the laminar burning speed and compare it to experimental data (see Fig. 1). The resulting spatial profiles of temperature, density, and species mass fractions are used to start a freely expanding flame in spherical coordinates (1D stretched). The initial

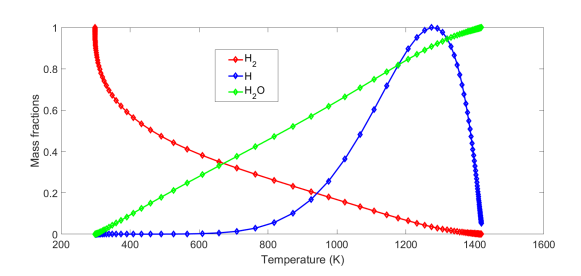


Figure 3: Comparison of the species mass fraction profiles vs temperature for the freely expanding flame at point C (lines) with the stationary flame profiles (symbols) at point E for H₂O, H₂ and H. Each mass fraction was normalized by its maximum value.

flame radius is set to $r_F \approx 4l_F$, which corresponds to $\kappa\tau_F \approx 2.2$. This corresponds to point A in Fig. 2. Equations 3-5 are solved until a normalized time of about $t/\tau_F \approx 10$. Initially, between points A and B, the flame exhibits a transient behavior due to the change from Cartesian to spherical coordinates. Then, from point B on, the flame speed decreases (at a rate that is related to the Markstein length), and the flame radius increases almost linearly.

At point C, after all transient effects have vanished, a new simulation is initiated corresponding to a stationary spherical flame . Equations 10-12 are solved with the analytical closure model for the flame stretch rate, κ , (Eq. 14). As intended, the flame radius and flame speed remain constant at the same values as for point C (black lines on Fig. 2). Figure 3 confirms that the species profiles are identical between the freely propagating flame results at point C and the stationary flame results at point E.

Finally, at point E, new simulations are started with different stretch values for the flame stretch rate, κ , de-

Analytical closure (Eq. 14)			Estimates	
H_2	O_2	H ₂ O	Eq. 15	Eq. 16
0.296	0.292	0.295	0.323	0.302

Table 1: Numerical values for the stretch rate κ at point C, normalized by τ_F , obtained with the analytical expression (Eq. 14) for different species and with the two estimates (Eq. 15 and Eq. 16).

viating by $\pm 3\%$ from the analytical closure expression (Eq. 14). As the imposed stretch does not correspond to the expected one at the radius of point E, the flame moves spatially and ultimately reaches a new steady state radius. Simulations with a smaller (resp. larger) stretch (-1% and -3%) have a larger (resp. smaller) final radius than point E. This change in stretch rates is associated with a change in the flame speed (see Fig. 2(b)); larger stretch rate values lead to larger flame speeds. The relationship between imposed stretch rate and final flame speed will be exploited later in section 5.

As mentioned in section 2.2.2, the analytical closure for the stretch rate, κ , can be evaluated from any reacting species (i.e., not N₂). As shown in Table 1, the numerical values obtained for H₂, O₂, and H₂O are very close to each other and vary by at most 1%. These differences were found to decrease with grid resolution, taking values of 0.72 and 0.37% for 40 and 80 grid points per flame thickness. Numerical values for the two estimates (Eq. 15 and Eq. 16) are also provided in Table 1. Taking into account the burnt gases within the flame is key for obtaining a precise approximation as Eq. (16) performs better than Eq. (15) (about 2% error vs. about 10%).

Finally, the chosen spatial resolution affects very slightly the calculation of S_L for a given κ . Discrepancies between the results for 20, 40, and 80 points per flame thickness do not exceed 1%.

5. Stretch effects

The previous section has shown that the new simulation framework (Eq. 10-12 with Eq. 14) produces stationary spherical flames that match exactly freely-expanding spherical flames. The next step is to leverage this new framework to study the impact of stretch rate on the laminar flame speed.

5.1. Extracting the Markstein length

As pointed out in the previous section, the laminar flame reaches a different steady-state radius and a different steady-state burning speed for each imposed stretch rate, κ . Figure 4 presents the steady state flame speeds (normalized by its unstretched value) for six different

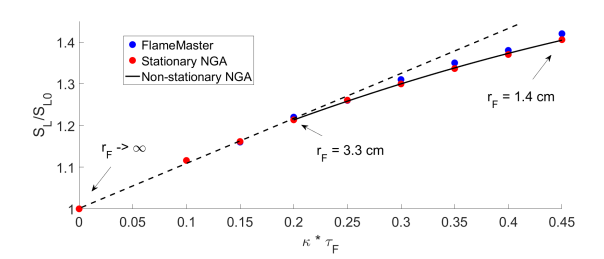


Figure 4: Evolution of the laminar flame speed normalized by the unstretched value at different normalized stretch rate values for stationary spherical flames in NGA (red symbols), FlameMaster (blue symbols), and for a freely propagating spherical flame (black lines). The dashed line represents a linear interpolation to zero stretch (Eq. 2).

imposed stretch rates (normalized by τ_F) for $\phi=0.4$. For these simulations, the fields were initialized with the flat/unstretched flame profiles, and r_F was estimated using Eq. (16). Also shown on the figure are the results of a freely-propagating spherical flame covering the same range of stretch rates. As the flame propagates outwardly, the flame radius increases (from $r_F=1.4\,\mathrm{cm}$ to $r_F=3.3\,\mathrm{cm}$)), and the stretch rate decreases (from 0.45 to 0.2). The results of the stationary spherical flames and the freely-propagating spherical flame are in excellent agreement for any given stretch rate.

As the stretch rate increases, the laminar flame speed increases. This dependence is characteristic of a negative Markstein length situation and is expected for lean hydrogen/air mixtures (here $\phi=0.4$). The Markstein length may be evaluated using Eq. 2 and fitting a linear function to the simulation results (dashed line in Fig. 4), resulting in $\mathcal{L}_M \approx -0.74$ mm.

5.2. Computational cost savings

This new methodology for obtaining \mathcal{L}_M not only provides accurate results, but it also yields considerable savings in computational cost. The non-stationary simulation (solid line in Fig. 4) was about 50 times more computationally expensive than any of the steady-state simulations (red dots in Fig. 4), all running on the same computer. This considerable saving is made possible by estimating *a priori* the stretch value for the desired flame radius (or vice versa) from Eqs. 15 or 16. Then, the (κ, r_F) data pair is used to generate initial profiles that quickly converge to the desired steady state. It is possible to decrease the computational cost further by reducing the domain only to a narrow range of radii around the flame front.

To this end, the proposed method has been incorporated in the steady-state solver FlameMaster [23]. The implementation consisted in converting the spatial

$\kappa au_{ m F}$	${ m S_L/S_L^0}$				
	$\phi = 0.4$	$\phi = 0.75$	$\phi = 1.0$	$\phi = 1.25$	
0.2	1.23	0.98	0.81	0.77	
0.3	1.31	0.94	0.75	0.69	
0.4	1.37	0.92	0.69	0.60	

Table 2: Numerical values for the normalized laminar burning velocity, S_L , for different values of normalized stretch rates, κ , for hydrogen/air mixtures at different equivalence ratios.

derivatives from Cartesian to spherical coordinates, and treating the source terms involving κ in Eqs. (10)-(12) as an additional advection term. Specifically, even though the gas velocity, u_r , is always positive, the effective advection velocity, $u_r - \frac{1}{2}\kappa r'$, is always negative. Hence, the unburnt side (end of the domain) is an inlet, and the burnt side is the outlet.

The FlameMaster results for the hydrogen case at $\phi = 0.4$ are shown in Fig. 4 and are in excellent agreement with the results obtained with the unsteady solver NGA. Using a dedicated steady-state solver with a non-uniform mesh leads to a dramatic computational cost reduction. Obtaining the solution requires a couple of intermediate simulations to converge to the desired point, each simulation running in a few seconds. In comparison, each stationary NGA simulation took a few minutes. Finally, the use of a non-uniform mesh optimized around the flame front further reduces the impact of the grid resolution. The flame speeds at $\kappa \tau_F = 0.35$ with 200 and 400 grid points differ by only 3%.

5.3. Comparison with experimental data

The procedure described above for a hydrogen/air mixture at $\phi = 0.4$ is repeated for three additional equivalence ratios ($\phi = 0.75$, 1.0, and 1.25). Table 2 provides the normalized flame speed obtained from stationary spherical flame simulations at three different normalized stretch rates ($\kappa \tau_F = 0.2, 0.3, \text{ and } 0.4$).

While the laminar flame speed increases with stretch rate for $\phi=0.4$, it is found to decrease for the other three cases. This is characteristic of a positive Markstein length. Using the lowest stretch rate, we estimate the burnt Markstein lengths to be $\mathcal{L}_M^b \approx +0.22\,\mathrm{mm}$, $+2.16\,\mathrm{mm}$, and $+2.72\,\mathrm{mm}$ for $\phi=0.75$, 1.0, and 1.25 respectively. These values are compared to experimental data in Fig. 5. The numerical values are in good agreement with the experimental results. The order of magnitude of the errors is acceptable taking into account the uncertainty in the extraction of Markstein length (up to 60 %) [15].

5.4. Extension to hydrocarbon/air mixtures

To show the generality of the method, we perform simulations for two additional fuels (CH₄ and n–C₇H₁₆) using the proposed framework. Following the methodology detailed in Section 5.1, we extract the Markstein length \mathcal{L}_M for different equivalence ratios. The results are shown in Figure 6 and are in very good agreement with experimental data. Opposite behaviors are predicted for the two fuels. For n-heptane, unlike methane and hydrogen, the Markstein length decreases as the mixture becomes richer, and the laminar flame speed becomes less sensitive to changes in the stretch rate. This is a typical characteristic of n-alkanes, for which negative \mathcal{L}_M can be obtained for rich mixtures [48].

6. Conclusions

In this work, we proposed a mathematical framework for the simulation of stationary spherical flames. The key element is a coordinate change to maintain the flame radius constant. The governing equations in the new flame-attached frame of reference resemble the original equations for freely-propagating spherical flames. The only difference is the presence of an additional source in

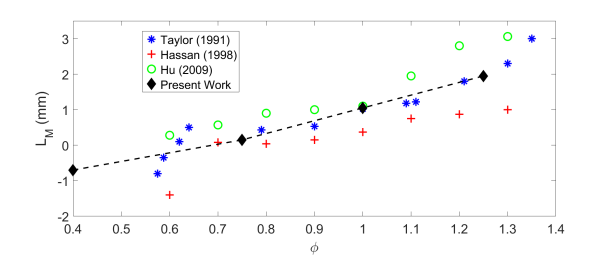


Figure 5: Comparison of the Markstein lengths extracted from stationary spherical flame simulations (black diamonds and dashed line) with experimental values (symbols) for different hydrogen mixtures [45–47]

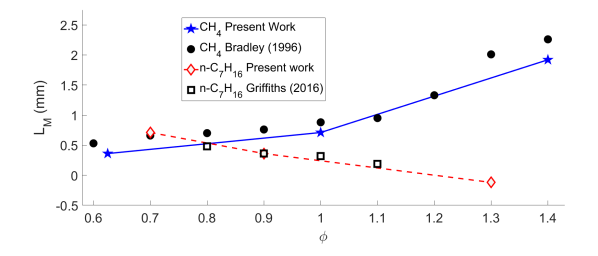


Figure 6: Comparison of the Markstein lengths extracted from stationary spherical flame simulations for CH_4 (filled blue symbols and solid line) and C_7H_{16} (open red symbols and dashed line) with experimental values (black symbols) for different equivalence ratios [24, 48]

each equation, whose purpose is to drive the numerical solution to a steady state. These source terms involve one free parameter: the flame stretch rate. This quantity may be computed in real time in an unsteady calculation in order to keep the flame radius constant. It could also be imposed. In this second case, the flame radius and flame speed adjust to match the imposed stretch rate.

The results of the stationary spherical flame simulations were found to match those of freely expanding spherical flame at a given stretch rate. This includes both global quantities (such as the flame speed) and species profiles. The dependence of the laminar flame speed on the stretch rate was leveraged to extract Markstein lengths for hydrogen/air mixtures at different equivalence ratios, as well as for hydrocarbon/air mixtures (CH₄ and n-C₇H₁₆). Numerical results were found to be in good agreement with experimental measurements (and within experimental uncertainties).

This proposed methodology is ideally suited for implementation in traditional steady-state chemical kinetic software such as Chemkin/Premix, Cantera, and FlameMaster, and removes the need for unsteady solvers. The use of a dedicated steady-state solver with a non-uniform mesh was found to lead to significant cost reductions over the use of an unsteady solver.

Acknowledgments

This material is based upon work supported by the National Science Foundation under Grant No. 1832548.

References

- [1] G. P. Smith, D. M. Golden, F. Frenklach, N. W. Moriarty, B. Eiteneer, M. Goldenberg, C. T. Bowman, R. K. Hanson, S. Song, W. C. J. Gardiner, V. V. Lissianski, Z. Qin, http://www.me.berkeley.edu/grimech/.
- [2] G. Blanquart, P. Pepiot-Desjardins, H. Pitsch, Chemical mechanism for high temperature combustion of engine relevant fuels with emphasis on soot precursors, Combustion and Flame 156 (2009) 588–607.
- [3] L. E. Bollinger, W. A. Strauss, R. Edse, Burning velocities of bunsen burner flames by the flame-pressure method, Industrial & Engineering Chemistry 49 (1957) 768–773.
- [4] C. Vagelopoulos, F. Egolfopoulos, C. Law, Further considerations on the determination of laminar flame speeds with the counterflow twin-flame technique, Symposium (International) on Combustion 25 (1994) 1341–1347.
- [5] K. Bosschaart, L. de Goey, The laminar burning velocity of flames propagating in mixtures of hydrocarbons and air measured with the heat flux method, Combustion and Flame 136 (2004) 261–269.
- [6] D. R. Dowdy, D. B. Smith, S. C. Taylor, A. Williams, The use of expanding spherical flames to determine burning velocities and stretch effects in hydrogen/air mixtures, Symposium (International) on Combustion 23 (1991) 325–332.

- [7] M. Matalon, B. J. Matkowsky, Flames as gasdynamic discontinuities, Journal of Fluid Mechanics 124 (1982) 239.
- [8] G. H. Markstein, Experimental and theoretical studies of flamefront stability, Journal of the Aeronautical Sciences 18 (1951) 199–209.
- [9] W. B. Bush, F. E. Fendell, Asymptotic analysis of laminar flame propagation for general lewis numbers, Combustion Science and Technology 1 (1970) 421–428.
- [10] P. Pelce, P. Clavin, Influence of hydrodynamics and diffusion upon the stability limits of laminar premixed flames, Journal of Fluid Mechanics 124 (1982) 219.
- [11] P. Clavin, Dynamic behavior of premixed flame fronts in laminar and turbulent flows, Progress in Energy and Combustion Science 11 (1985) 1–59.
- [12] J. Tien, M. Matalon, On the burning velocity of stretched flames, Combustion and Flame 84 (1991) 238–248.
- [13] P. Ronney, G. Sivashinsky, A theoretical study of propagation and extinction of nonsteady spherical flame fronts, SIAM Journal on Applied Mathematics 49 (1989) 1029–1046.
- [14] Z. Chen, X. Qin, B. Xu, Y. Ju, F. Liu, Studies of radiation absorption on flame speed and flammability limit of CO2 diluted methane flames at elevated pressures, Proceedings of the Combustion Institute 31 (2007) 2693–2700.
- [15] F. Wu, W. Liang, Z. Chen, Y. Ju, C. K. Law, Uncertainty in stretch extrapolation of laminar flame speed from expanding spherical flames, Proceedings of the Combustion Institute 35 (2015) 663–670.
- [16] S. Davis, C. Law, Laminar flame speeds and oxidation kinetics of iso-octane-air and n-heptane-air flames, Symposium (International) on Combustion 27 (1998) 521–527.
- [17] A. Kelley, C. Law, Nonlinear effects in the extraction of laminar flame speeds from expanding spherical flames, Combustion and Flame 156 (2009) 1844–1851.
- [18] E. R. Hawkes, J. H. Chen, Comparison of direct numerical simulation of lean premixed methane–air flames with strained laminar flame calculations, Combustion and Flame 144 (2006) 112– 125
- [19] B. Savard, G. Blanquart, Broken reaction zone and differential diffusion effects in high karlovitz n-c7h16 premixed turbulent flames, Combustion and Flame 162 (2015) 2020–2033.
- [20] C. Xiouris, T. Ye, J. Jayachandran, F. N. Egolfopoulos, Laminar flame speeds under engine-relevant conditions: Uncertainty quantification and minimization in spherically expanding flame experiments. Combustion and Flame 163 (2016) 270–283.
- [21] R. Kee, F. Rupley, J. Miller, CHEMKIN-II: a FORTRAN chemical kinetics package for the analysis of gas-phase chemical kinetics, Technical Report, Sandia National Laboratories, CA, 1989.
- [22] D. G. Goodwin, R. L. Speth, H. K. Moffat, B. W. Weber, Cantera: An object-oriented software toolkit for chemical kinetics, thermodynamics, and transport processes, https://www.cantera.org. Version 2.4.0.
- [23] H. Pitsch, FlameMaster: a C++ computer program for 0D combustion and 1D laminar flame calculations (1998).
- [24] D. Bradley, P. Gaskell, Burning velocities, markstein lengths, and flame quenching for spherical methane-air flames: A computational study, Combustion and Flame 104 (1996) 176–198.
- [25] T. Poinsot, D. Veynante, Theoretical and Numerical Combustion, Edwards, p. 79.
- [26] O. Desjardins, G. Blanquart, G. Balarac, H. Pitsch, High order conservative finite difference scheme for variable density low mach number turbulent flows, Journal of Computational Physics 227 (2008) 7125–7159.
- [27] M. Herrmann, G. Blanquart, V. Raman, Flux corrected finite volume scheme for preserving scalar boundedness in reacting

- large-eddy simulations, AIAA Journal 44 (2006) 2879-2886.
- [28] R. B. Bird, W. E. Stewart, E. N. Lightfoot, Transport phenomena, John Wiley Sons, 2007.
- [29] R.B.Bird, J.O.Hirschfelder, C.F.Curtiss, Molecular theory of gases and liquids, John Wiley Sons, 1964.
- [30] S. Lapointe, B. Savard, G. Blanquart, Differential diffusion effects, distributed burning, and local extinctions in high karlovitz premixed flames, Combustion and Flame 162 (2015) 3341–3355.
- [31] J. H. Ferziger, H. G. Kaper, E. P. Gross, Mathematical theory of transport processes in gases, American Journal of Physics 41 (1973) 601–603.
- [32] S. Mathur, P. Tondon, S. Saxena, Thermal conductivity of binary, ternary and quaternary mixtures of rare gases, Molecular Physics 12 (1967) 569–579.
- [33] Z. Hong, D. F. Davidson, R. K. Hanson, An improved H2/O2 mechanism based on recent shock tube/laser absorption measurements, Combustion and Flame 158 (2011) 633–644.
- [34] K.-Y. Lam, D. F. Davidson, R. K. Hanson, A shock tube study of H2+OH → H2O + H using OH laser absorption, International Journal of Chemical Kinetics 45 (2013) 363–373.
- [35] Z. Hong, K.-Y. Lam, R. Sur, S. Wang, D. F. Davidson, R. K. Hanson, On the rate constants of OH+HO2 and HO2+HO2: A comprehensive study of H2O2 thermal decomposition using multi-species laser absorption, Proceedings of the Combustion Institute 34 (2013) 565–571.
- [36] M. M. Fabrizio Bisetti, Guillaume Blanquart, H. Pitsch, Combustion and Flame 159 (2012) 317–335.
- [37] F. Egolfopoulos, C. Law, An experimental and computational study of the burning rates of ultra-lean to moderately-rich h2/o2/n2 laminar flames with pressure variations, Symposium (International) on Combustion 23 (1991) 333–340.
- [38] S. Tse, D. Zhu, C. Law, Morphology and burning rates of expanding spherical flames in H2/O2/inert mixtures up to 60 atmospheres, Proceedings of the Combustion Institute 28 (2000) 1793–1800.
- [39] N. Lamoureux, N. Djeballi-Chaumeix, C.-E. Paillard, Laminar flame velocity determination for H2-air-He-CO2 mixtures using the spherical bomb method, Experimental Thermal and Fluid Science 27 (2003) 385–393.
- [40] A. K. Das, K. Kumar, C.-J. Sung, Laminar flame speeds of moist syngas mixtures, Combustion and Flame 158 (2011) 345–353.
- [41] V. A. Alekseev, M. Christensen, E. Berrocal, E. J. Nilsson, A. A. Konnov, Laminar premixed flat non-stretched lean flames of hydrogen in air, Combustion and Flame 162 (2015) 4063–4074.
- [42] M. Giannakopoulos, A. Gatzoulis, C. Frouzakis, Consistent definitions of "flame displacement speed" and "markstein length" for premixed flame propagation, Combustion and Flame 162 (2015) 1249–1264.
- [43] M. Matalon, J. Bechtold, The dependence of the markstein length on stoichiometry, Combustion and Flame 127 (2001) 1906–1913.
- [44] G. Giannakopoulos, C. Frouzakis, S. Mohan, A. Tomboulides, M. Matalon, Consumption and displacement speeds of stretched premixed flames - theory and simulations, Combustion and Flame 208 (2019) 164–181.
- [45] S. Taylor, Burning Velocity and the Influence of Flame Stretch, Ph.D. thesis, University of Leeds, 1991.
- [46] M. Hassan, Burning Velocity and the Influence of Flame Stretch, Combustion and Flame - Burning Velocity and the Influence of Flame Stretch (1998) 539–550.
- [47] E. Hu, Z. Huang, J. He, C. Jin, J. Zheng, Experimental and numerical study on laminar burning characteristics of premixed methane–hydrogen–air flames, International Journal of Hydrogen Energy 34 (2009) 4876–4888.

[48] R. G. John Griffiths, R. Woolley, Turbulent burning rates of gasoline components, part 2 – effect of carbon number, Fuel 167 (2016)